Emergent Form-Finding for Center of Mass Control of Ball-Shaped Tensegrity Robots

Kyunam Kim[1], Adrian K. Agogino[2], and Alice M. Agogino[1]

[1] University of California at Berkeley, Berkeley CA 94720, USA,
{knkim,agogino}@berkeley.edu,
WWW home page: http://best.berkeley.edu/drupal/tensegrity
[2] University of California at Santa Cruz, Santa Cruz CA 95064, USA,
adrian.k.agogino@nasa.gov

Abstract. Controls for ball-shaped robots based on tensegrity structures (built from pure tension and compression elements, i.e., interconnected cables and rods), have gained significant capabilities including the ability to roll, go up-hill and climb over obstacles. These gains have been made possible through the use of machine learning and physics simulations that allow controls to be "learned" instead of being engineered in a top-down fashion. While effective, these methods unfortunately give little insight into how these learned control methods accomplish their goals nor do they give us insight as to the robustness of the control strategy. These robustness issues have shown to be especially problematic when applied to physical robots; small errors between simulation and hardware have prevented the physical robots from rolling. This paper describes how these shortcomings can be addressed in three ways: 1) We present a dynamic relaxation technique that describes the shape of a tensegrity structure given the forces on its cables; 2) We then show how control of a tensegrity robot "ball" can be decomposed into finding its shape and then determining the center of mass and supporting polygon for this new shape; 3) Using a multi-step Monte Carlo algorithm, we determine the structural geometry that pushes the center of mass out of the supporting polygon to provide the most robust basic mobility step that can lead to rolling. Combined these elements will give greater insight into the control process, provide an alternative to the existing physics simulations and offer a greater degree of robustness in terms of bridging the gap between simulation and hardware.

Keywords: tensegrity structures, evolutionary algorithm, monte carlo, dynamic relaxation

1 Introduction

Tensegrity structures are a unique class of structures constructed by a network of cables connecting isolated rods [11, 24]. The way these structures distribute forces across their members has many analogies to multi-agent systems and networks [15]. Although no rod members touch each other, a tensegrity structure

maintains its equilibrium geometry by delicately balancing cable tension and rod compression forces. In other words, rod ends, or *nodes*, where cables are connected, of a tensegrity structure at an equilibrium experience zero net forces. This property of the structure is exploited in Sect. 2, where an equilibrium of the structure is found by a dynamic relaxation technique.

Naturally compliant tensegrity structures have several advantages for soft robotic platforms. For example, they are lightweight, robust, energy efficient and capable of a wide range of motions [30, 28, 27, 29]. Moreover, their structural compliance allow them to work beside humans safely. For this reason, tensegrity robots have been envisioned for assistive and rehabilitative healthcare by providing hospital service or direct in-home assistance. Furthermore, U.S. National Aeronautics and Space Administration (NASA) is developing tensegrity robots for space exploration missions [1, 32, 7, 26]. Since multiple tensegrity robots can often be packed into a small volume, NASA has been investigating using multiple cooperative tensegrity robots for planetary missions [14].

However, to operate tensegrity robots in such applications, they should have mobility. In the literature, simulations as well as physical demonstrations of locomotion of several tensegrity robots have been introduced [21, 23, 7, 10, 5, 25, 6, 4, 3, 9, 19, 13]. In these works, it was shown that different modes of locomotion such as rolling, crawling and undulating are possible with tensegrity robots, depending on their structural geometry. Among many possible tensegrity geometries, our work focuses on a six-strut ball-shaped tensegrity robot. This work aims to develop a control for the structural deformation of the tensegrity robot to enable its mobility.

1.1 Six-Strut Tensegrity Robots

Six-strut tensegrity robots are based on an expandable octahedron tensegrity structure with 6 rigid rods and 24 cables. Each node is connected to 4 neighbor nodes by cables and 1 neighbor node by a rod. An example of our rapidly prototyped six-strut tensegrity robot is shown in Fig. 1. This robot is cable-driven and fully actuated, meaning that all 24 cables are independently actuated by linear actuators located at the centers of the edges. The most natural choice of locomotion method for this ball-shaped robot is a discontinuous motion we call "punctuated rolling." A six-strut tensegrity robot can realize such motion by continuously deforming its geometry by actuating its cables or rods or both [25, 7, 6, 17, 9, 19].

In Koizumi et al. [19], a six-strut tensegrity robot equipped with 24 pneumatic actuators was introduced and its control strategy for rolling was presented. The work tested all possible single and double actuator policies with varying air pressure applied to the actuators, and identified the policies that allowed the robot to perform controlled punctuated rolling motions, or *steps*. Later, the authors developed a dynamics model of the robot and simulated its motion by numerically integrating the obtained equations of motion [12]. Furthermore, by using this model, they have found a couple of double actuator policies which

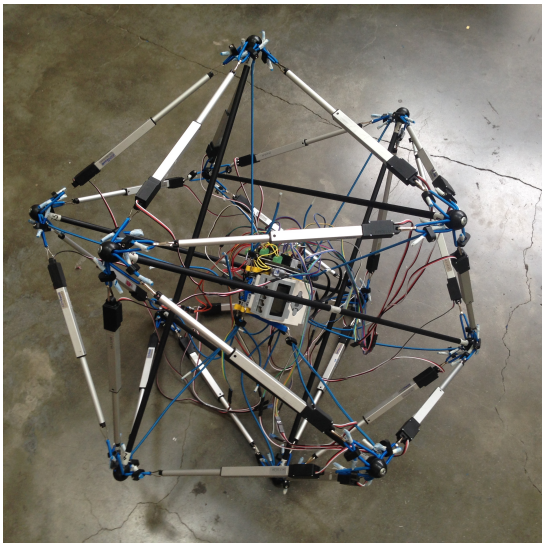

Fig. 1. Rapidly prototyped six-strut tensegrity robot at UC Berkeley.

allowed stepping of their robot. While the basic structure of the pneumatically-actuated robot is identical to our rapidly prototyped robot (Fig. 1), there was a fundamental difference between the two robots that did not allow direct implementation of the previously mentioned actuation polices to our robot. That is, the former was tethered to an external air compressor to supply high air pressure to the pneumatic actuators, which enabled the robot to quickly deform its body to a large extent. Our robot, on the other hand, is completely untethered, and the choice of actuators is limited by multiple factors, such as weight, power consumption and physical dimensions. As a result, the stroke length, speed of actuation and maximum force provided by the actuators are also limited, and the way our robot is deformed is dissimilar to the pneumatically-actuated robot. This motivated us to further develop actuation policies that better suit our robot. Moreover, the aforementioned works identified actuation policies involving up to only two actuators per step. By using more actuators and thus achieving greater deformation of the robot, it is probable that more reliable steps can be performed. For this reason, this work aims to identify policies that use all 24 actuators per step.

In general, dynamic models of tensegrity systems are quite complicated as they have high degrees of freedoms and complex interactions between their members [22, 12, 31, 27, 29, 16, 16]. Therefore, it is often non-trivial to obtain analytical models of tensegrity systems and integrate them to simulate their motions. To overcome this difficulty, an alternative approach using physics engine simulators for simulating the motions of tensegrity systems has been proposed [8, 7, 21, 10, 15, 14, 9]. This approach not only enables real-time simulations of tensegrity systems but also facilitates the development of controllers for their loco-

motion. However, since these physics engine simulators are *approximating* the exact dynamics of tensegrity systems, a validation step is required to verify their simulated results [7, 14]. Furthermore, because the simulators codify all of the underlying physics, it can be hard to obtain a physical interpretation for the simulated results, let alone gain insights as to how to control the robots.

In this work, instead of simulating the complicated dynamics of a six-strut tensegrity robot, we develop the controller for stepping of the robot based on a simple physical observation: the robot will perform a step if its ground projection of the center of mass (GCoM) is pushed outside of its supporting polygon. As a consequence, our goal is to find deformations of the robot structure that satisfy this condition. Moreover, the step will be more reliable if GCoM is farther away from the supporting polygon. Another condition that should be met is that the deformed structural geometries must also be in equilibrium states, that is, all nodes should experience zero net forces. To achieve the latter condition, we propose a dynamic relaxation technique which finds an equilibrium configuration of the robot structure associated with the given actuation policy. Furthermore, we propose a multi-step Monte Carlo sampling method to find equilibrium configurations that also satisfy the former condition.

In the authors' previous work, different motions, including forward movement and turning, of a six-strut tensegrity robot were developed by performing multiple controlled punctuated rolling motions [17]. In this prior work, the target geometry was found with the help of a search algorithm, and it was assumed that cables could only be in one of two possible states: full extension or retraction. Considering that there are total of 24 cables on the structure, this assumption results in 2^{24} possible states of the structure. If the assumption is slightly modified and each cable is allowed to have n multiple states, then the total number of possible states of the structure grows exponentially, n^{24}. In such a huge state space, looking for a desired geometry with a search method could be challenging and inefficient. To overcome this difficulty, an evolutionary approach with Monte Carlo sampling is used in this work to find a target geometry of the robot for performing a step. A similar approach was presented in [21, 20] where the controllers of tensegrity robots were parameterized first and the best performing sets of parameters were identified with a multi-step Monte Carlo. While these works deal with repetitively oscillating controllers for generating continuous locomotion of tensegrity robots in simulation, our work focuses on the controller design achieving discretized basic motions of our physical robot.

The outline of the work is as follows. In Sect. 2, a form-finding problem of a six-strut tensegrity structure is discussed and a dynamic relaxation technique is applied to find an equilibrium of the structure given an initial structural geometry and imbalanced member forces. In Sect. 3, a Monte Carlo approach for sampling of a set of six-strut tensegrity equilibrium configurations is described. The sampled equilibria are then evaluated based on a fitness function to be defined later. An evolutionary algorithm which runs multiple generations of Monte Carlo sampling is presented in Sect. 4. Section 5 shows our simulation results of the aforementioned procedure. Finally, conclusions are provided in Sect. 6.

2 Form-Finding by Dynamic Relaxation

The purpose of dynamic relaxation (DR) is to find an equilibrium configuration of a cable net structure in an iterative way, starting from an initial configuration that does not necessarily satisfy the force balance condition [2, 33]. External forces applied to the structure may also be considered in the form-finding process. This section describes how DR is used to find an equilibrium of a six-strut tensegrity structure.

DR can further be subdivided into two different methods, depending on the type of damping used during iterations. The first method uses viscous damping, while the other uses kinetic damping. In this work, the kinetic damping method is used as it has been shown to be stable with good convergence properties for systems with large local disturbances, which is the case for tensegrity structures [2].

DR with kinetic damping is based on Newton's second law. Consider a node i ($i = 1, \cdots, 12$) and assume a force $\mathbf{F}_i(t)$ is applied to the node. Note that the force is a function of time. If we denote the nodal mass as m_i, then the motion of the node is governed by Newton's second law.

$$\mathbf{F}_i(t) = m_i \dot{\mathbf{v}}_i(t) \ . \tag{1}$$

In the above equation, $\mathbf{v}_i(t)$ is the velocity of node i at time t. Using the centered finite difference form of the velocity, the acceleration $\dot{\mathbf{v}}_i(t)$ can be approximated.

$$\dot{\mathbf{v}}_i(t) = \frac{\mathbf{v}_i(t + \Delta t/2) - \mathbf{v}_i(t - \Delta t/2)}{\Delta t} \ . \tag{2}$$

Substituting (2) into (1) gives an iterative form of velocity update.

$$\mathbf{v}_i(t + \Delta t/2) = \mathbf{v}_i(t - \Delta t/2) + \frac{\Delta t}{m_i}\mathbf{F}_i(t) \ . \tag{3}$$

In (3), m_i has a fictitious value, that is, the mass may or may not come from an actual physical system. Usually, m_i and Δt are tuned for good convergence of the algorithm [2]. Therefore, if the total force applied to node i at time t, $\mathbf{F}_i(t)$, is known, the velocity of the node can be updated for the next time step.

The position of node i can also be updated using the updated velocity.

$$\mathbf{r}_i(t + \Delta t) = \mathbf{r}_i(t) + \mathbf{v}_i(t + \Delta t/2)\Delta t \ . \tag{4}$$

In (4), $\mathbf{r}_i(t)$ is the position of node i at time t.

DR is an iterative method that aims to find an equilibrium of the structure from an initial configuration which may be given arbitrarily. That is, the initial nodal positions $\mathbf{r}_i(0)$ for all i may be chosen arbitrarily. Furthermore, the initial nodal velocities are set to zero in DR, that is, $\mathbf{v}_i(0) = \mathbf{0}$ for all i. Because the centered finite difference form is used for the velocity, (3) is slightly modified for the first velocity update.

$$\mathbf{v}_i(\Delta t/2) = \frac{\Delta t}{2m_i}\mathbf{F}_i(0) \ . \tag{5}$$

In summary, if the initial configuration of the structure is known and the total nodal forces are tracked over time, then the nodal positions and velocities can be computed for the later time steps iteratively.

In DR with kinetic damping, kinetic energy of the system is tracked over time.

$$\mathrm{KE}(t) = \sum_{i=1}^{12} \frac{1}{2} m_i \mathbf{v}_i(t) \cdot \mathbf{v}_i(t) \ . \tag{6}$$

When the peak of the kinetic energy is detected, then all of the nodal velocities and nodal forces are set to zero, and this is what it means by *kinetic damping*. By taking this step, energy is dissipated from the system, moving the system towards local minimum energy state, or an equilibrium. The iteration restarts from the beginning with the new initial configuration defined as the latest configuration at the energy peak. Finally, the whole process is repeated until the kinetic energy as well as the sum of all nodal force magnitudes converge to zero within an error bound. At convergence, the final configuration is regarded as an equilibrium. An example plot of changes of kinetic energy and sum of all nodal force magnitudes over time is shown in Fig. 2.

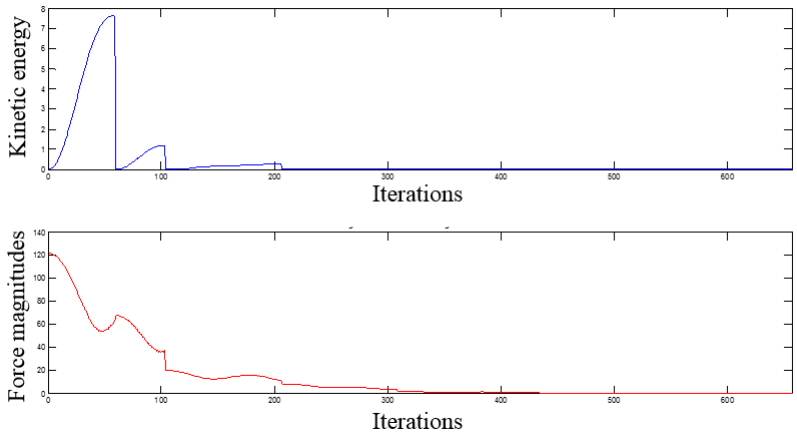

Fig. 2. An example of changes of kinetic energy and nodal force magnitudes over time while running DR. Notice that both values converge to zero, meaning that an equilibrium is found.

It is noted here that, because of the way DR finds an equilibrium, the intermediate states do not necessarily represent the actual physical behavior of the structure. It is only the final equilibrium configuration that has a physical meaning.

2.1 Nodal Forces

The nodal force $\mathbf{F}_i$ consists of three different types of forces.

1. $\mathbf{F}_i^s$: Spring forces applied by cables connected to the node.
2. $\mathbf{F}_i^a$: Applied forces by external sources such as actuators.
3. $\mathbf{F}_i^r$: A constrained force applied by a connected rod to maintain constant length of the rod.

The total nodal force is then the sum of all three forces.

$$\mathbf{F}_i(t) = \mathbf{F}_i^s(t) + \mathbf{F}_i^a(t) + \mathbf{F}_i^r(t) \ . \tag{7}$$

Let $J^i = \{i_1, \cdots, i_4\}$ represent a set of neighbor nodes that are connected to node i by cables. Then, at each time step t, the spring force $\mathbf{F}_i^s(t)$ applied to node i is the sum of individual cable forces.

$$\mathbf{F}_i^s(t) = \sum_{j \in J^i} F_{ij}^s(t) \frac{\mathbf{r}_j(t) - \mathbf{r}_i(t)}{\|\mathbf{r}_j(t) - \mathbf{r}_i(t)\|} \ . \tag{8}$$

$$F_{ij}^s(t) = \begin{cases} k(\|\mathbf{r}_j(t) - \mathbf{r}_i(t)\| - l_0) & \text{if } \|\mathbf{r}_j(t) - \mathbf{r}_i(t)\| > l_0 \\ 0 & \text{if } \|\mathbf{r}_j(t) - \mathbf{r}_i(t)\| \leq l_0 \ . \end{cases} \tag{9}$$

In the above equations, cables are assumed to be linearly elastic and can only bear tensile forces in tensegrity structures. Therefore, when their lengths become smaller than their rest lengths, the cable forces are set to zero. In (9), k and l_0 are cable stiffness and rest length, respectively, and are assumed to have the same constant values for all cables in this work.

$\mathbf{F}_i^a(t)$ is the sum of forces applied to node i from external sources such as actuators. In a cable-driven tensegrity robot, actuators pull or release cables to provide additional forces to the cables. Therefore, the directions of actuation forces are always parallel to those of the cables.

$$\mathbf{F}_i^a(t) = \sum_{j \in J^i} F_{ij}^a(t) \frac{\mathbf{r}_j(t) - \mathbf{r}_i(t)}{\|\mathbf{r}_j(t) - \mathbf{r}_i(t)\|} \ . \tag{10}$$

In this work, the actuation forces are assumed to be constant over time, that is, $F_{ij}^a(t) = F_{ij}^a = F_{ji}^a$. The magnitudes of these forces can be chosen arbitrarily as long as they remain in a physically acceptable range. In Sect. 3, multiple instances of F_{ij}^a are sampled from a uniform distribution, and an equilibrium configuration corresponding to these sampled actuation forces is found and evaluated.

The last type of force applied to node i is a rod constraint force, $\mathbf{F}_i^r(t)$. This force does not appear in pure tensile structures and is a unique feature of tensegrity structures. It is critical to obtain the correct expression for this force, as it guarantees the constant distance between two end nodes of a rigid rod, and therefore, stability of the whole tensegrity structure. In order to find an

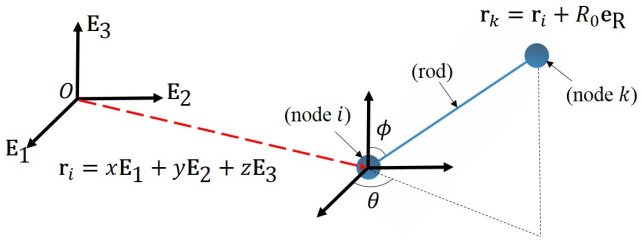

Fig. 3. Coordinate systems used for describing kinematics of two end nodes of a rod.

expression for a rod constraint force, the coordinate systems shown in Fig. 3 are used. Here, the position of the first end node of a rod is described by a Cartesian coordinate system, while the position of the other node is described relative to the first one by using a spherical coordinate system. Then, the following equations describe the constraint force of a single rod acting on its end nodes i and k.

$$\mathbf{F}_i^r(t) = -F_{ik}^r(t)\mathbf{e}_\mathbf{R}(t), \quad \mathbf{F}_k^r(t) = F_{ik}^r(t)\mathbf{e}_\mathbf{R}(t) \ . \tag{11}$$

$$\begin{aligned} F_{ik}^r(t) = m_k\big[&\ddot{x}\sin(\phi)\cos(\theta) + \ddot{y}\sin(\phi)\sin(\theta) + \ddot{z}\cos(\phi) \\ &-R_0\dot{\phi}^2 - R_0\dot{\theta}^2\sin^2(\phi)\big] - (\mathbf{F}_k^s + \mathbf{F}_k^a)\cdot\mathbf{e}_\mathbf{R} \ . \end{aligned} \tag{12}$$

In (12), m_k and R_0 are mass of node k and rod length, respectively. The coordinates x, y, z, ϕ and θ as well as the forces $\mathbf{F}_k^s$ and $\mathbf{F}_k^a$ are functions of time, but their notations are omitted for better readability of the equation. Because the nodal positions $\mathbf{r}_i(t)$ and $\mathbf{r}_k(t)$ as well as the nodal velocities $\mathbf{v}_i(t)$ and $\mathbf{v}_k(t)$ are updated iteratively using (3) and (4), the angular coordinates $\phi(t)$ and $\theta(t)$ and their derivatives $\dot{\phi}(t)$ and $\dot{\theta}(t)$ can also be updated using coordinate transformations. Moreover, the acceleration of node i,

$$\mathbf{a}_i(t) = \dot{\mathbf{v}}_i(t) = \ddot{x}(t)\mathbf{E}_1 + \ddot{y}(t)\mathbf{E}_2 + \ddot{z}(t)\mathbf{E}_3 \ . \tag{13}$$

is already given by (2). As a result, the rod constraint force $\mathbf{F}_i^r(t) = -\mathbf{F}_k^r(t)$ can be updated over time.

Our simulations showed that, when the rod constraint forces were appropriately applied, the maximum error in rod lengths was 0.14% while running DR.

3 Monte Carlo Sampling of Equilibrium Configurations

In Sect. 2, DR with kinetic damping is used to find an equilibrium of a six-strut tensegrity structure when an initial configuration and applied forces are given. Clearly, different initial conditions will result in different equilibria. Some of these equilibria will allow the robot to make a step from one supporting

polygon to another, while the others will not. A condition for this to happen is to place the ground projection of the structure's center of mass (GCoM) outside of its supporting polygon. The goal of this section is to find equilibrium configurations that satisfy the preceding condition. In this work, Monte Carlo sampling approach is used for this purpose.

Among the three types of forces described in Sect. 2.1, one that is controlled to deform the actual robot structure is externally applied actuation forces. Since a six-strut tensegrity structure has a total of 24 cables, if a cable-driven tensegrity robot is fully actuated, maximally 24 external forces from actuators can be added to the cables independently. Denoting a vector of all actuation forces as $\mathbf{F}^a(t)$,

$$\mathbf{F}^a(t) = \mathbf{F}^a = \left[\cdots, F^a_{ij} = F^a_{ji}, \cdots\right] \in \mathbb{R}^{24} \quad . \\ \text{for all pairs of nodes } (i,j) \text{ connected by cables} \tag{14}$$

As discussed in Sect. 2.1, these forces are parallel to cable directions at all times, and their magnitudes, $F^a_{ij} = F^a_{ji}$, are assumed to be constant while running DR. Therefore, if initial magnitudes of these forces are known, then the forces can be fully prescribed for all of the later time steps. It is this force vector $\mathbf{F}^a$ that are sampled and altered in different DR executions. Each component of the vector is sampled independently from a uniform distribution within a physically acceptable range. For each sampled vector of actuation force magnitudes, DR with kinetic damping is performed from an initial configuration of a regular icosahedron, and resulting equilibrium configuration is found. Each equilibrium is then evaluated according to a fitness function described in Sect. 3.1. This process is repeated over a large number of samples. Finally, the best equilibrium configuration of the pool and the force vector sample that produced this equilibrium are identified.

3.1 Evaluation

As discussed in Sect. 1.1, in order to make a step from a six-strut tensegrity robot, its GCoM should be placed outside of its supporting polygon. Assuming masses are uniformly distributed in rods and cables have negligible masses, the center of mass of the structure can be easily obtained once nodal positions at an equilibrium are known. To evaluate each equilibrium, the center of mass is projected onto all of the planes of the outer surface triangles of the structure. There are two types of triangles on the outer surface of the structure: (a) 8 closed triangles each of which is enclosed by 3 cables and (b) 12 open triangles each of which is enclosed by only 2 cables. Since in most cases the robot steps to and from a closed triangle [17], only this type of triangles are considered when evaluating an equilibrium. That is, the center of mass is projected onto 8 different planes which closed triangles lie in. For each projection, the distances between the projected point and 3 edges of a closed triangle are measured, as shown in Fig. 4. If the projected point crosses over an edge and moves outside of a triangle, that distance is measured as a negative value. Because the structural

geometry should push GCoM as far as possible from a supporting polygon for a reliable step, our goal is to minimize this distance towards a large negative value. For this reason, 24 distances are computed per equilibrium (3 distances per triangle, 8 closed triangles) and the minimum of these values is assigned as a score for that configuration. Finally, among a set of equilibrium configurations, the one with the minimum score is picked as the best configuration of the set.

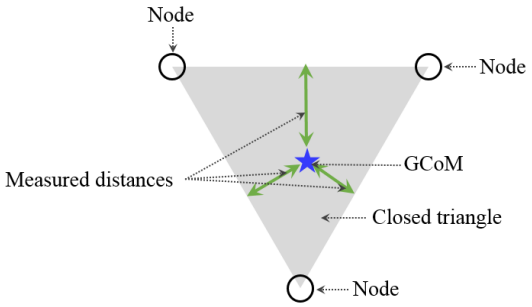

Fig. 4. Distances measured between GCoM and three triangle edges.

4 Evolutionary Algorithm

Due to the high dimensionality of sampled force vectors $\mathbf{F}^a$ and the wide interval of the sampling space, finding an equilibrium with a negative score from a single set of samples is highly unlikely. One way to improve the method and find equilibria with negative scores is to perform sampling and evaluation for multiple generations sequentially. To improve scores of samples over generations, sampling of input force vectors for a generation happens in a nearby region of the force vector that resulted in the best scoring equilibrium in the previous generation.

For the samples of the first generation, components of input force vectors, ${}_1\mathbf{F}^a$, where the left subscript denotes its generation, are all sampled from a uniform distribution of the same range, $[f_{min}, f_{max}]$, where f_{min} and f_{max} represent minimum and maximum magnitudes of forces that can be applied by actuators. Once all samples of the first generation are obtained and evaluated according to the fitness function defined in Sect. 3.1, the equilibrium configuration with minimum score, ${}_1\bar{\mathcal{C}}$, as well as the force vector sample that produced this equilibrium, ${}_1\bar{\mathbf{F}}^a$, are identified. The bar notation represents the sample being optimal in current generation.

For subsequent generations, say generation j ($j = 2, 3, \cdots$), input force vectors, ${}_j\mathbf{F}^a$, are sampled around the best force vector of the previous generation, ${}_{j-1}\bar{\mathbf{F}}^a$. Specifically, multiples of ${}_j\mathbf{F}^a$ are sampled from a uniform distribution of

$[{}_{j-1}\bar{\mathbf{F}}^a - \delta\mathbf{F},\ {}_{j-1}\bar{\mathbf{F}}^a + \delta\mathbf{F}]$, where $\delta\mathbf{F}$ is a 24 dimensional constant vector. Once the pre-determined number of samples are created and evaluated at generation j, the equilibrium with minimum score, ${}_j\bar{\mathcal{C}}$, as well as the force vector, ${}_j\bar{\mathbf{F}}^a$, producing this equilibrium are found. In generation $(j+1)$, input force vectors are sampled around the force vector ${}_j\bar{\mathbf{F}}^a$ in a similar manner, and the process is repeated until termination conditions are met or the pre-defined maximum number of generations is reached.

5 Simulation Results

In order to find a desired geometry of a six-strut tensegrity robot, which pushes GCoM out of a supporting polygon and allows a step, 20 generations were run sequentially with the procedure described in Sect. 4. Each generation contained 100 samples. In our simulations, physical parameters were adopted from our rapidly prototyped tensegrity robot, Fig. 1. The parameter values used for simulations are summarized in Table 1.

Table 1. Parameters Used for Simulation

Rod length (R_0)	0.69 m
Cable rest length (l_0)	0.341 m
Cable stiffness (k)	450 N/m
Actuator force range ($[f_{min}, f_{max}]$)	[0 N, 45 N]
Constant force vector ($\delta\mathbf{F}$)	$[5, \cdots, 5]^{\mathrm{T}} \in \mathbb{R}^{24}$
Nodal mass (m_i)	1
Time step (Δt)	0.001

Figures 5 through 8 show intermediate results of this process. The first of these figures show scores of all samples of related generations, and the latter figures show distributions of the scores. It can be clearly seen from these figures that both the average and minimum scores of generations decrease as generations evolve. Figure 9 explicitly shows this behavior. Although the minimum score of the first generation has a large positive value, the score decreases as generations evolve, and becomes negative at generation 13. The score then saturates for the last few generations. The minimum score of all the generations occured at generation 19, and the equilibrium configuration corresponding to this score is shown in Fig. 10 in different perspectives. The score for this configuration is found to be -0.0079, which means this most desirable configuration placed its GCoM 0.0079 m (or 1.14% of the rod length R_0) outside of its supporting polygon. Once this desirable final configuration is found, either a position controller that regulates lengths of cables or a force controller that controls cable tensions can be developed to deform the structure to this target configuration.

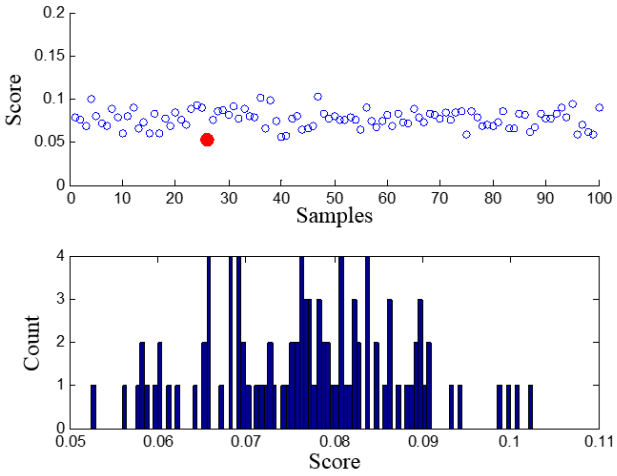

Fig. 5. Score distribution of 100 samples of generation 1. Red dot represents a sample with minimum score.

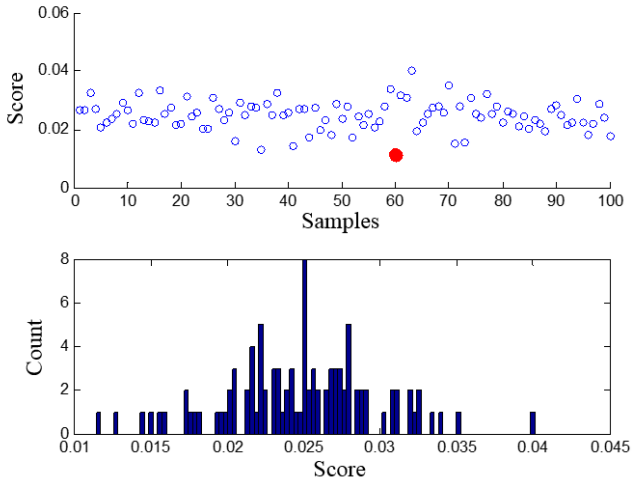

Fig. 6. Score distribution of 100 samples of generation 5. Red dot represents a sample with minimum score.

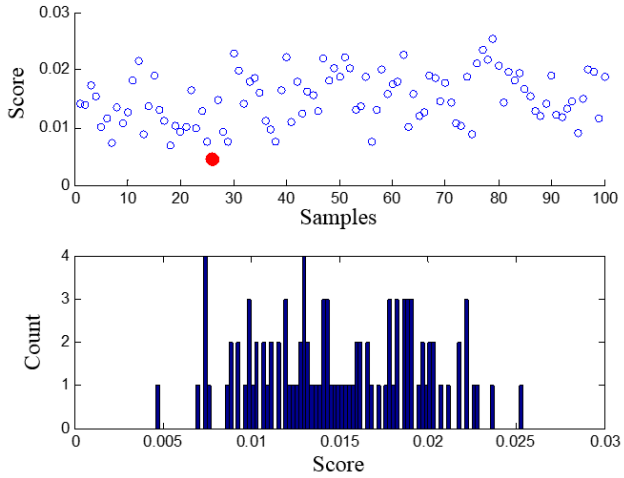

Fig. 7. Score distribution of 100 samples of generation 10. Red dot represents a sample with minimum score.

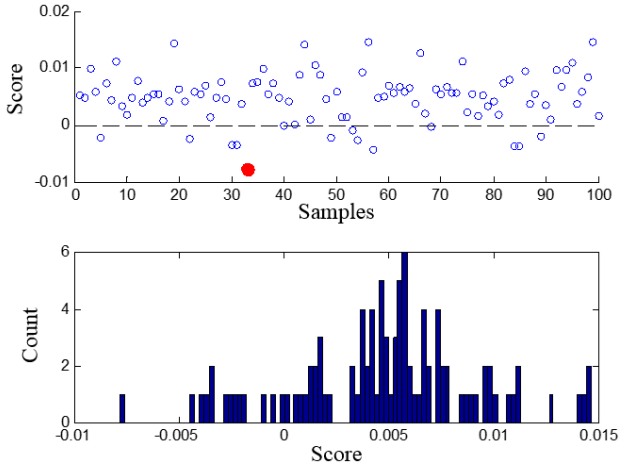

Fig. 8. Score distribution of 100 samples of generation 19. Red dot represents a sample with minimum score.

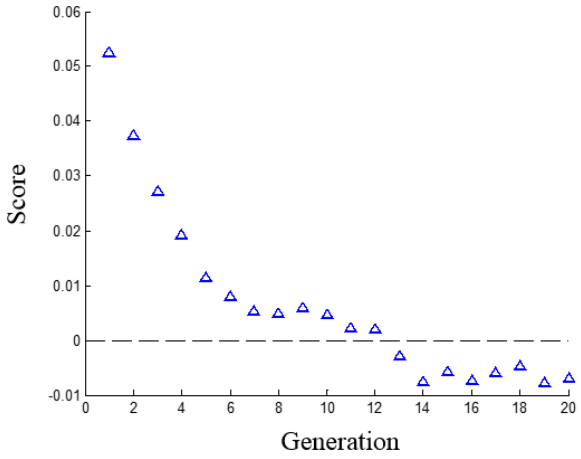

Fig. 9. Evolution of minimum scores over generations.

Our ongoing work focuses on development of a better model of our hardware robot, improvement of the simulation result with a more sophisticated fitness function and an increased number of samples, and implementation of the simulated results on the robot. Our preliminary results show that the simulated deformation is not only realizable with the hardware robot but also allows the robot to perform desired steps successfully [18]. The deformation of the hardware robot following the simulation result is presented in Fig. 11.

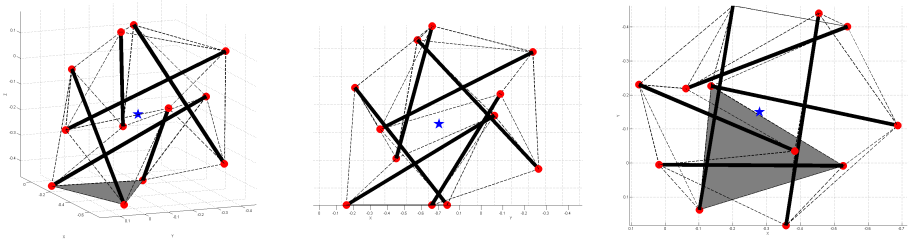

Fig. 10. An equilibrium geometry with the lowest score, ${}_{19}\bar{\mathcal{C}}$. Thick lines, thin dashed lines, red dots, blue stars and gray triangles represent rods, cables, nodes, center of masses and supporting polygons, respectively. Left: Perspective view. Middle: Side view. Right: Top view.

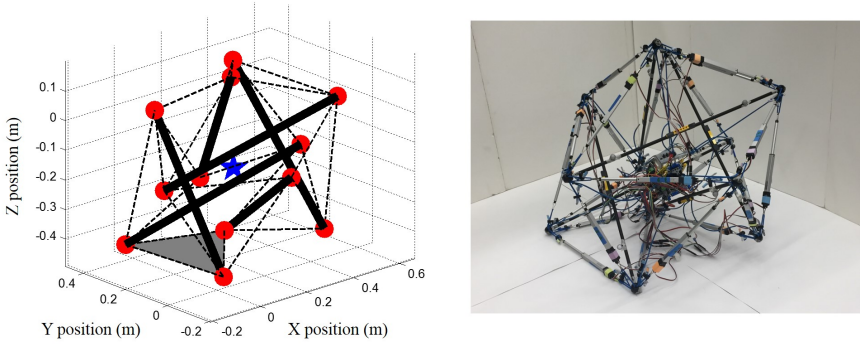

Fig. 11. Deformation of the hardware robot based on the simulation result.

6 Conclusions

In this work, a series of methods are presented, with the goal of finding a desired geometry of a six-strut tensegrity robot that allows it to make a step by shifting its GCoM outside of a supporting polygon. At the lowest level, DR with kinetic damping is used to find an equilibrium of the structure from an initial configuration with the consideration of constant actuation forces. In the midst of the procedure, a set of actuation force vectors are sampled uniformly within a physically acceptable range and DR is performed for all of the sampled cases, creating a pool of equilibria. At the highest level, an evolutionary algorithm is run, which creates multiple generations of equilibrium configurations. The algorithm improves the quality of samples as generations evolve by adjusting the sampling range using information obtained from samples of the previous generation. A set of simulations was run based on these methods using physical parameters taken from the rapidly prototyped six-strut tensegrity robot at UC Berkeley. The simulation results show that the quality of samples is, in fact, improved as generations proceed. Moreover, a desired geometry for stepping the robot is found after several generations. Once this equilibrium configuration is known, either a position or force feedback controller can be used to deform the robot structure to the target configuration by providing an appropriate amount of forces to the cables from actuators, which will enable the robot to perform a controlled step.

References

1. Agogino, A.K., SunSpiral, V., Atkinson, D.: Super Ball Bot – structures for planetary landing and exploration. NASA Innovative Advanced Concepts (NIAC) Program, Final Report (Jul 2013)
2. Barnes, M.R.: Form finding and analysis of tension structures by dynamic relaxation. International journal of space structures 14(2), 89–104 (1999)

3. Boehm, V., Jentzsch, A., Kaufhold, T., Schneider, F., Becker, F., Zimmermann, K.: An approach to locomotion systems based on 3d tensegrity structures with a minimal number of struts. In: Robotics; Proceedings of ROBOTIK 2012; 7th German Conference on. pp. 1–6. VDE (2012)
4. Bohm, V., Zimmermann, K.: Vibration-driven mobile robots based on single actuated tensegrity structures. In: Robotics and Automation (ICRA), 2013 IEEE International Conference on. pp. 5475–5480. IEEE (2013)
5. Bruce, J., Caluwaerts, K., Iscen, A., Sabelhaus, A.P., SunSpiral, V.: Design and evolution of a modular tensegrity robot platform. In: Robotics and Automation (ICRA), 2014 IEEE International Conference on (2014)
6. Bruce, J., Sabelhaus, A., Chen, Y., Lu, D., Morse, K., Milam, S., Caluwaerts, K., Agogino, A.M., SunSpiral, V.: SUPERball: Exploring tensegrities for planetary probes. In: Proceedings of 12th International Symposium on Artificial Intelligence, Robotics and Automation in Space (i-SAIRAS 2014). Montreal, Canada (Jun 2014)
7. Caluwaerts, K., Despraz, J., Işçen, A., Sabelhaus, A.P., Bruce, J., Schrauwen, B., SunSpiral, V.: Design and control of compliant tensegrity robots through simulation and hardware validation. Journal of The Royal Society Interface 11(98) (2014), http://dx.doi.org/10.1098/rsif.2014.0520
8. Center, N.A.R.: NASA tensegrity robotics toolkit. http://irg.arc.nasa.gov/tensegrity/NTRT/
9. Du, W., Ma, S., Li, B., Wang, M., Hirai, S.: Dynamic simulation for 6-strut tensegrity robots. In: Information and Automation (ICIA), 2014 IEEE International Conference on. pp. 870–875 (July 2014)
10. Friesen, J.M., Pogue, A., Bewley, T., de Oliveira, M., Skelton, R.E., SunSpiral, V.: A compliant tensegrity robot for exploring duct systems. In: Robotics and Automation (ICRA), 2014 IEEE International Conference on. Hong Kong (Jun 2014)
11. Fuller, B.: Tensegrity. Portfolio Artnews Annual 4, 112–127 (1961)
12. Hirai, S., Imuta, R.: Dynamic simulation of six-strut tensegrity robot rolling. In: Robotics and Biomimetics (ROBIO), 2012 IEEE International Conference on. pp. 198–204. IEEE (2012)
13. Hirai, S., Koizumi, Y., Shibata, M., Wang, M., Bin, L.: Active shaping of a tensegrity robot via pre-pressure. In: Advanced Intelligent Mechatronics (AIM), 2013 IEEE/ASME International Conference on. pp. 19–25. IEEE (2013)
14. Iscen, A.: Multiagent learning for locomotion and coordination in tensegrity robotics. Ph.D. thesis, Oregon State University (May 2014)
15. Iscen, A., Agogino, A., SunSpiral, V., Tumer, K.: Robust distributed control of rolling tensegrity robot. In: The Autonomous Robots and Multirobot Systems (ARMS) Workshop at AAMAS. vol. 2013 (2013)
16. Kanchanasaratool, N., Williamson, D.: Modelling and control of class nsp tensegrity structures. International Journal of Control 75(2), 123–139 (2002)
17. Kim, K., Agogino, A.K., Moon, D., Taneja, L., Toghyan, A., Dehghani, B., SunSpiral, V., Agogino, A.M.: Rapid prototyping design and control of tensegrity soft robot for locomotion. In: Proceedings of 2014 IEEE International Conference on Robotics and Biomimetics (ROBIO2014). Bali, Indonesia (Dec 2014)
18. Kim, K., Agogino, A.K., Toghyan, A., Moon, D., Taneja, L., Agogino, A.M.: Robust learning of tensegrity robot control for locomotion through form-finding. In: Berkeley Emergent Space Tensegrities (BEST) Lab working paper: 15-0301. UC Berkeley (2015)

19. Koizumi, Y., Shibata, M., Hirai, S.: Rolling tensegrity driven by pneumatic soft actuators. In: Robotics and Automation (ICRA), 2012 IEEE International Conference on. pp. 1988–1993. IEEE (2012)
20. Lessard, S., Agogino, A.K.: Multi-level monte carlo control algorithms to maneuver tensegrity robots out of obstacles. In: To appear in Proceedings of AAMAS 2015. AAMAS (2015)
21. Mirletz, B.T., Park, I.W., Flemons, T.E., Agogino, A.K., Quinn, R.D., SunSpiral, V.: Design and control of modular spine-like tensegrity structures. In: Proceedings of The 6th World Conference of the International Association for Structural Control and Monitoring (6WCSCM). Barcelona, Spain (Jul 2014)
22. Murakami, H.: Static and dynamic analyses of tensegrity structures. part 1. nonlinear equations of motion. International Journal of Solids and Structures 38(20), 3599–3613 (2001)
23. Paul, C., Valero-Cuevas, F.J., Lipson, H.: Design and control of tensegrity robots for locomotion. Robotics, IEEE Transactions on 22(5), 944–957 (2006)
24. Pugh, A.: An introduction to tensegrity. Univ of California Press (1976)
25. Sabelhaus, A.P., Bruce, J., Caluwaerts, K., Chen, Y., Lu, D., Liu, Y., Agogino, A.K., SunSpiral, V., Agogino, A.M.: Hardware design and testing of SUPERball, a modular tensegrity robot. In: Proceedings of The 6th World Conference of the International Association for Structural Control and Monitoring (6WCSCM). Barcelona, Spain (Jul 2014)
26. Sabelhaus, A.P., Bruce, J., Caluwaerts, K., Manovi, P., Firoozi, R.F., Dobi, S., Agogino, A.M., SunSpiral, V.: System design and locomotion of SUPERball, an autonomous tensegrity robot. In: To Appear in Proceedings of 2015 International Conference on Robotics and Automation (ICRA2015). Seattle, Washington (May 2015)
27. Skelton, R.: Dynamics and control of tensegrity systems. In: IUTAM Symposium on Vibration Control of Nonlinear Mechanisms and Structures. pp. 309–318. Springer (2005)
28. Skelton, R.E., Adhikari, R., Pinaud, J.P., Chan, W., Helton, J.: An introduction to the mechanics of tensegrity structures. In: Decision and Control, 2001. Proceedings of the 40th IEEE Conference on. vol. 5, pp. 4254–4259. IEEE (2001)
29. Skelton, R.E., de Oliveira, M.C.: Tensegrity systems. Springer (2009)
30. Skelton, R.T., Sultan, C.: Controllable tensegrity: A new class of smart structures. In: Smart Structures and Materials' 97. pp. 166–177. International Society for Optics and Photonics (1997)
31. Sultan, C.: Modeling, design, and control of tensegrity structures with applications. Ph.D. thesis, Purdue University (April 1999)
32. SunSpiral, V., Gorospe, G., Bruce, J., Iscen, A., Korbel, G., Milam, S., Agogino, A.K., Atkinson, D.: Tensegrity based probes for planetary exploration: Entry, descent and landing (EDL) and surface mobility analysis. International Journal of Planetary Probes (2013)
33. Zhang, L., Maurin, B., Motro, R.: Form-finding of nonregular tensegrity systems. Journal of Structural Engineering 132(9), 1435–1440 (2006)